Korean J. Chem. Eng., 35(6), 1247-1256 (2018)
DOI: 10.1007/s11814-018-0045-5

pISSN: 0256-1115
eISSN: 1975-7220

Effect of vertically varying permeability on the onset of convection in a porous medium

Won Sun Ryoo* **and Min Chan Kim****,†**

*Department of Chemical Engineering, Hongik University, Seoul 04066, Korea
**Department of Chemical Engineering, Jeju National University, Jeju 63243, Korea
(*Received 6 January 2018 • accepted 12 March 2018*)

Abstract−Considering the vertically varying permeability of a porous medium, we conducted theoretical and numerical analyses on the onset of buoyancy-driven instability in an initially quiescent, fluid-saturated, horizontal porous layer. Darcy's law was employed to explain the fluid flow through a porous medium and linear and nonlinear analyses are conducted. In the semi-infinite domain, the growth of disturbance and the onset of convection were analyzed with and without the quasi-steady state approximation. The present analysis of initial growth rate shows that the system is initially unconditionally stable regardless of a vertical heterogeneity parameter. The onset conditions of buoyancy-driven instabilities were investigated as a function of the Darcy-Rayleigh number and the heterogeneity parameter. To find the effect of a vertical heterogeneity on the flow after the onset of convection, nonlinear numerical simulations also were conducted using the result of the linear analysis as a starting point. Nonlinear numerical simulations show that the finger-like instability motion is not readily observable at a critical time and it becomes visible approximately when a mass transfer rate substantially increases.

Keywords: Buoyancy-driven Convection, Onset Condition, Vertically Heterogeneous Porous Medium, Linear Stability Analysis, Direct Numerical Simulation

INTRODUCTION

The analysis of convective instability in a porous medium begins with Horton-Rogers-Lapwood (HRL) convection [1,2]. They examined thermally driven convection and used the methods developed for convection in a homogeneous fluid. The extension of the classical HRL convection by considering the heterogeneity of a porous medium is well-reviewed by Nield and Bejan [3]. The above mentioned studies assumed that there was a linear increase in temperature with depth, appropriate for gradual heating or for a steady state. Adopting the methods developed for a homogeneous fluid layer, Caltagirone [4] first analyzed the effect of the transient base temperature field on the incipient convection in a porous medium.

Recently, in connection with the carbon dioxide (CO_2) sequestration, the transient HRL convection has been extensively studied [5]. Although the density increase for CO_2 is only around 1% at subsurface conditions, on long time scales this can lead to a convective mixing process, which significantly accelerates the dissolution of CO_2. Furthermore, this convective motion can enhance the efficient usage of the lower parts of aquifer, because the high-density water saturated with CO_2 will flow downward and be replaced by less saturated water with lower density. Ennis-King et al. [5] and Xu et al. [6] extended Caltagirone's [4] analysis into anisotropic porous media, and Hassanzadeh et al. [7] considered the various initial and boundary condition effects. Later, Rapaka et al. [8] revisited this problem by introducing non-modal stability theory and provided a structural history of the most unstable disturbances. The above-mentioned studies solve the stability equation in a layer of uniform thickness. However, in the CO_2 dissolution process, the aquifer in contact with CO_2 layer across the upper free boundary can be treated as a semi-infinite in the vertical direction. Considering this situation, Riaz et al. [9], Selim and Rees [10] and Wessel-Berg [11] analyzed the onset of convection in porous media under the time-dependent temperature or concentration field in the semi-infinite domain. They claimed that their analysis in the semi-infinite domain yields accurate stability criteria since the basic fields have the boundary-layer characteristics. Also, the stability of time dependent base states has been investigated by energy method [4-6] and its modification [12]. Riaz and Cinar [13] give a good review on the modelling of the solubility trapping of CO_2 in an isotropic porous medium.

Since sedimentary rocks generally have a vertically heterogeneous structure, which is important in geological applications. However, less attention has been given to the effect of the vertically variable permeability on the onset of gravitational instabilities. Rapaka et al. [14] considered the effect of a permeability variation in the vertical direction on the amplification of the perturbation which is introduced at time t=0. They also analyzed the effect of a horizontally anisotropic permeability. In addition, Nield and Kuznetsov [15] extended the time-dependent stability analysis to an anisotropic system. Later, conducting nonlinear numerical simulations, Ranganathan et al. [16] and Kong and Saar [17] analyzed the effect of heterogeneous porous medium on the CO_2 geological storage. Hill and Morad [18] considered the effect of vertical anisotropy on the

†To whom correspondence should be addressed.
E-mail: mckim@cheju.ac.kr

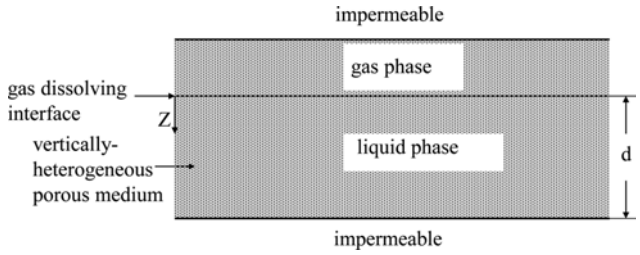

Fig. 1. Schematic diagram of system considered here.

onset of gravitational instabilities in a geochemical reaction system.

In the present study, the incipient behavior of buoyancy-driven convection in a porous medium whose permeability is vertically varying is investigated by using the linear analysis. A new set of stability equations was derived in the semi-infinite domain and finite one, and solved with and without the quasi-steady state approximation (QSSA). Through the analysis of initial growth rate, the most dangerous mode of disturbance was identified. The critical conditions for the onset of buoyancy-driven convection were investigated as a function of the Darcy-Rayleigh number and the heterogeneity parameter. Based on the results of the linear stability analysis, the nonlinear evolution of convective motion was analyzed through the direct numerical simulation (DNS) study.

SYSTEM AND GOVERNING EQUATIONS

The system of interest is an initially quiescent, fluid-saturated, horizontal porous layer of depth d, as shown in Fig. 1. Initially the fluid layer contains no solute: C=0 at t=0. For time t≥0, gas starts to dissolve into fluid layer across the upper free boundary which is assumed to be maintained at uniform concentration C_i. The lower boundary is assumed to be impermeable with no mass flux condition. The standard governing equations for solute-driven convective mixing consist of Darcy's law for the fluid motion in a porous medium and the convective diffusion equation for the transport of the dissolved solute. Under the Boussinesq approximation, they can then be written as follows [18]:

$$\nabla\cdot\mathbf{U}=0, \tag{1}$$

$$\mathbf{U}=-\frac{\mathbf{K}}{\mu}\cdot(\nabla P+\beta\mathbf{g}C), \tag{2}$$

$$\varepsilon\frac{\partial C}{\partial t}+\mathbf{U}\cdot\nabla C=\varepsilon\mathcal{D}\nabla^2 C, \tag{3}$$

where **U** is the Darcy velocity vector, μ is the fluid viscosity, **K** is the absolute permeability matrix, P is the hydrostatic potential, **g** is the gravitational acceleration, ε is the porosity, C is the solute concentration, t is time, β is the volumetric expansion coefficient and $\mathcal{D}$ is the effective diffusivity of the solute in the aqueous phase in the porous medium. In the present study, the permeability is assumed to be isotropic but depth-dependent, and therefore matrix **K** has following form:

$$\mathbf{K}=K(Z)\mathbf{I}, \tag{4}$$

where **I** is 3×3 identity matrix. The key parameters to describe the present system are the Darcy-Rayleigh number Ra and the permeability function F(Z) defined by

$$Ra=\frac{g\beta K_0 C_i d}{\varepsilon\mathcal{D}\nu} \text{ and } F(Z)=\frac{K(Z)}{K_0},$$

where K_0 is the permeability at Z=0 and Z is the vertical coordinate along the gravity direction.

For a system having vertically varying permeability, the critical time t_c to represent the onset of buoyancy-driven motion remains controversial. For this transient stability analysis, a set of nondimensionalized variables z, τ and c_0 is defined by using the scale of vertical length l(=d/Ra), time $l^2/(\varepsilon\mathcal{D})$, and concentration C_i. Then the basic conduction state is described in non-dimensionalized form by

$$\frac{\partial c_0}{\partial\tau}=\frac{\partial^2 c_0}{\partial z^2}, \tag{5}$$

with the following initial and boundary conditions,

$$c_0(0,z)=0,\ c_0(\tau,0)=1,\ \text{and}\ \left.\frac{\partial c_0}{\partial z}\right|_{(\tau,Ra)}=0 \tag{6a, b & c}$$

The above equations can be solved by using the conventional separation of variables technique as follows [5]:

$$c_0(\tau,z)=1-\frac{2}{\pi}\sum_{n=1}^{\infty}\frac{2}{2n-1}\sin\left\{\left(\frac{2n-1}{2}\right)\frac{\pi z}{Ra}\right\}\exp\left[-\left\{\left(\frac{2n-1}{2}\right)\frac{\pi}{Ra}\right\}^2\tau\right]. \tag{7}$$

For the extreme case of $\sqrt{\tau}/Ra\to 0$, the solution to the above equation can be given as [19]

$$c_0(\tau,z)=\mathrm{erfc}\left(\frac{\zeta}{2}\right), \tag{8}$$

where $\zeta=z/\sqrt{\tau}$. Furthermore, Kim and Choi [19] showed that the similarity solution (8) represent the exact one (7) quite well for the case of $\sqrt{\tau}/Ra<0.1$.

LINEAR STABILITY ANALYSIS

1. Stability Equations

According to the linear stability theory, by disturbing Eqs. (1)-(3), the dimensionless disturbance equations can be formulated as

$$\nabla^2 w_1-\frac{d\ln f}{dz}\frac{dw_1}{dz}=f\nabla_1^2 c_1, \tag{9}$$

$$\frac{\partial c_1}{\partial\tau}+w_1\frac{\partial c_0}{\partial z}=\nabla^2 c_1, \tag{10}$$

where $\nabla^2=\frac{\partial^2}{\partial x^2}+\frac{\partial^2}{\partial y^2}+\frac{\partial^2}{\partial z^2}$, $\nabla_1^2=\frac{\partial^2}{\partial x^2}+\frac{\partial^2}{\partial y^2}$ and f(z)=F(Z/*l*). Here, c_1 and w_1 are the dimensionless concentration and vertical velocity disturbances, respectively. Lengths in lateral *x*- and *y*-directions have the scale of *l*. In addition, the vertical velocity component has the scale of $\varepsilon\mathcal{D}/l$ and the concentration component has the scale of C_i. The proper boundary conditions are given by

$$w_1=c_1=0 \text{ at } z=0, \tag{11a}$$

$$w_1=\frac{\partial c_1}{\partial z}=0 \text{ at } z=Ra. \tag{11b}$$

The above boundary conditions indicate no flow across the boundaries and the fixed concentration on the upper boundary and the mass flux condition of the lower boundary.

Based on the Fourier-mode analysis, convective motion is assumed to exhibit the horizontal periodicity [20]. Then the perturbed quantities can be expressed as products of two separate terms:

$$\{w_1(\tau, x, y, z), c_1(\tau, x, y, z)\}=\{w_1(\tau, z), c_1(\tau, z)\}\exp\{i(k_x x+k_y y)\}, \tag{12}$$

where "i" is the imaginary number. Substituting the above Eq. (12) into Eqs. (9)-(10) produces the following usual amplitude functions in terms of the horizontal wave number $k=(k_x^2+k_y^2)^{1/2}$:

$$\left(\frac{d^2}{dz^2}-k^2\right)w_1-\frac{d\ln f}{dz}\frac{dw_1}{dz}=-k^2 f c_1, \tag{13}$$

$$\frac{\partial c_1}{\partial \tau}=\left(\frac{\partial^2}{\partial z^2}-k^2\right)c_1-w_1\frac{\partial c_0}{\partial z}, \tag{14}$$

under the boundary conditions (11). Although Hill and Morad [18], Harfash and Hill [21] assumed $f=1+(\gamma d/Ra)z$ with $|\gamma|<1$ to ensure $f>0$, for the mathematical convenience, we use the following simple relation in the present study:

$$f=\exp\left(-\frac{\delta d}{Ra}z\right). \tag{15}$$

Harfash [22] also employed this relation in his stability analysis. Equation (15) and Hill and Morad's [18] relation correspond to $K(Z)=K_0\exp(-\delta Z)$ and $K(Z)=K_0(1+\gamma Z)$, respectively. For the case of small δ, Eq. (15) represents Hill and Morad's [18] relation with $\delta=-\gamma$.

For $(\sqrt{\tau}/Ra)<<1$, the system is equivalent to a deep pool system, and therefore, the onset time is independent of the vertical extent of the system. Ben et al. [23] and Riaz et al. [9] discussed that the vertical diffusional operator, $\partial^2/\partial z^2$, does not have localized eigenfunctions for the deep pool system. Thus, the disturbances which are localized near the diffusion front cannot be accurately captured in the global (τ, z)-domain. Applying a coordinate transformation to the similarity variable of the base state $\zeta=z/\sqrt{\tau}$, the disturbance equations can be expressed as

$$\left(\frac{\partial^2}{\partial \zeta^2}+\delta^*\frac{\partial}{\partial \zeta}-k^{*2}\right)w_1=-\exp(-\delta^*\zeta)k^{*2}c_1, \tag{16}$$

$$\tau\frac{\partial c_1}{\partial \tau}+\sqrt{\tau}w_1\frac{\partial c_0}{\partial \zeta}=\left(\frac{\partial^2}{\partial \zeta^2}+\frac{\zeta}{2}\frac{\partial}{\partial \zeta}-k^{*2}\right)c_1, \tag{17}$$

under the following boundary conditions:

$$w_1=c_1=0 \text{ at } \zeta=0, \tag{18a}$$

$$w_1\to 0 \text{ and } c_1\to 0 \text{ as } \zeta\to\infty. \tag{18b}$$

where $\delta^*=(\delta d/Ra)\sqrt{\tau}$ and $k^*=k\sqrt{\tau}$. Note that the transformation to the semi-infinite domain by $(\tau, z)\to(\tau, \zeta)$ is singular at $\tau=0$. Hence, the temporal evolution of the disturbance must be kept away from the singular limit of $\tau=0$. In any case, any semi-infinite domain solution produces the unrealistic limit of the infinite gradient or amplitude at $\tau=0$.

2. Initial Growth Rate

At an initial stage of $t\to 0$, by neglecting higher order terms in τ, Eqs. (16) and (17) can be simplified to

$$\frac{\partial}{\partial \zeta}\left\{\exp(\delta^*\zeta)\frac{\partial w_1}{\partial \zeta}\right\}=0, \tag{19}$$

$$\tau\frac{\partial c_1}{\partial \tau}+\sqrt{\tau}w_1\frac{\partial c_0}{\partial \zeta}=\left(\frac{\partial^2}{\partial \zeta^2}+\frac{\zeta}{2}\frac{\partial}{\partial \zeta}\right)c_1, \tag{20}$$

under the boundary conditions (18). Based on Eq. (19), the solution of the velocity disturbance can be expressed as

$$w_1=d_1\int_0^\zeta \exp(-\delta^*\xi)d\xi+d_2. \tag{21}$$

Here the constants d_1 and d_2 should be zero to meet the boundary conditions (18). Since $w_1\to 0$ as $\tau\to 0$, the stability equation for the initial stage becomes

$$\tau\frac{\partial c_1}{\partial \tau}=\mathcal{L}_\zeta c_1, \tag{22}$$

where

$$\mathcal{L}_\zeta=\frac{\partial^2}{\partial \zeta^2}+\frac{\zeta}{2}\frac{\partial}{\partial \zeta}. \tag{23}$$

Because Eq. (22) is linear and homogeneous, using the generalized Fourier series c_1 can be expressed as

$$c_1(\tau, \zeta)=\sum_{n=1}^{\infty}a_n(\tau)\kappa_n\phi_n(\zeta), \tag{24}$$

where $\kappa_n[=\{2^{n-1/2}\pi^{1/4}\sqrt{\Gamma(2n)}\}^{-1}]$ is the normalization factor and $\Gamma(\cdot)$ is the gamma function. $\{\phi_n(\zeta)\}$ is the set of eigenfunctions of the following Sturm-Liouville equation:

$$\mathcal{L}_\zeta\phi_n=-\lambda_n\phi_n, \tag{25}$$

under the following boundary conditions:

$$\phi_n(0)=0 \text{ and } \phi_n|_{\zeta\to\infty}\to 0. \tag{26}$$

The solution of the above problem, Eqs. (25) and (26), is

$$\phi_n=\kappa_n H_{2n-1}\left(\frac{\zeta}{2}\right)\exp\left(-\frac{\zeta^2}{4}\right), \tag{27a}$$

$$\lambda_n=n=1, 2, \ldots, \tag{27b}$$

where H_k is the k-th Hermite polynomial. The above eigenfunctions are orthonormal, since

$$\int_0^\infty \kappa_i\kappa_j\phi_i\phi_j\exp\left(\frac{\zeta^2}{4}\right)d\zeta=\delta_{ij}, \tag{28}$$

where $\exp(\zeta^2/4)$ is the weighting function of the Sturm-Liouville Eq. (25) and δ_{ij} is the Kronecker delta. Then, the temporal evolution of the amplitude functions are governed by

$$\tau\frac{da_n}{d\tau}=-\lambda_n a_n. \tag{29}$$

The above result implies that at the early state of sufficiently small time, all modes of disturbance decay as τ^{-n} for n=1, 2, ⋯. For sufficiently small time, as discussed in the Riaz et al's work [9], the disturbance having the greatest growth rate is

$$c_1=a_1(\tau)\kappa_1\phi_1(\zeta)=\frac{1}{\sqrt{2\sqrt{\pi}}}a_1(\tau)\zeta\exp\left(-\frac{\zeta^2}{4}\right), \tag{30}$$

This is a fascinating structure for the amplitude function of disturbance at the initial state. Riaz et al. [9] derived this disturbance for the long-wave limit of k→0 and called it the dominant mode disturbance.

To trace the growth of the disturbance, the norm of the disturbance $\|c_1\|$ is defined as

$$\|c_1\|=\left\{\int_0^\infty |c_1|^2\exp\left(\frac{\zeta^2}{4}\right)d\zeta\right\}^{1/2}=\sqrt{\mathbf{a}^T\mathbf{a}}, \tag{31}$$

where $\mathbf{a}=[a_1, a_2, \cdots]$ and $\mathbf{a}^T$ is the transpose of **a**. By using this quantity, the growth rate σ^* can be defined as

$$\sigma^*=\frac{1}{\|c_1\|}\frac{d\|c_1\|}{d\tau}=\frac{1}{2\mathbf{a}^T\mathbf{a}}\left(\frac{d\mathbf{a}^T}{d\tau}\mathbf{a}+\mathbf{a}^T\frac{d\mathbf{a}}{d\tau}\right). \tag{32}$$

Then, the growth rate of this most unstable disturbance of Eq. (30) is

$$\sigma^*\tau=-1 \text{ as } \tau\to 0. \tag{33}$$

This means that the system is initially stable for the disturbance of the present study because the growth rate of the most unstable disturbance is negative. Kim and Choi [24] showed that the initial growth rate relation (33) is maintained even if we use the standard l^2-norm rather than the present Eq. (31).

TIME EVOLVING SOLUTIONS

1. Spectral Analysis

Here, the linear stability Eqs. (16)-(18) are tried to be solved by spectral method. From Eqs. (16) and (24), w_1 is expressed as

$$w_1=\sum_{n=1}^{\infty}a_n(\tau)\kappa_n\psi_n(k^*, \zeta), \tag{34}$$

and ψ_n's can be obtained by solving

$$(D^2+\delta^*D-k^{*2})\psi_n=-\exp(-\delta^*\zeta)k^{*2}\phi_n, \tag{35}$$

under the following boundary conditions:

$$\psi_n(0)=\psi_n(\infty)=0, \tag{36}$$

where $D=d/d\zeta$. The solution of Eqs. (35) and (36) is

$$\psi_n=-\frac{k^{*2}}{\sqrt{\delta^{*2}+4k^{*2}}}\left[\begin{array}{l}\exp(\alpha_1\zeta)\int_0^\zeta\exp(\alpha_2\xi)\phi_n(\xi)d\xi\\ -\exp(-\alpha_2\zeta)\int_0^\zeta\exp(\alpha_1\xi)\phi_n(\xi)d\xi\\ -\int_0^\infty\exp(\alpha_2\xi)\phi_n(\xi)d\xi\{\exp(\alpha_1\zeta)\\ -\exp(-\alpha_2\zeta)\}\end{array}\right], \tag{37}$$

where $\alpha_1=(-\delta^*+\sqrt{\delta^{*2}+4k^{*2}})/2$ and $\alpha_2=(-\delta^*-\sqrt{\delta^{*2}+4k^{*2}})/2$. By calculating the integrals in Eq. (37), the above solution can be expressed as the following recursive forms:

$$\psi_n=4\alpha_2^2\psi_{n-1}-4k^{*2}[\exp(-\delta^*\zeta)\phi_{n-1}(\zeta)+\delta^*\omega_{n-1}], \tag{38a}$$

$$\omega_n=4\alpha_1^2\omega_{n-1}-4\alpha_1\exp(-\delta^*\zeta)\phi_{n-1} -2\exp\left(-\frac{\zeta^2}{4}-\delta^*\zeta\right)H_{2n-2}\left(\frac{\zeta}{2}\right)+2H_{2n-2}(0)\exp(\alpha_2\zeta), \tag{39a}$$

with

$$\psi_1=-\frac{2k^{*2}\sqrt{\pi}}{\sqrt{\delta^{*2}+4k^{*2}}}\left[\begin{array}{l}\alpha_2\exp(\alpha_2^2)\left\{\mathrm{erf}\left(\frac{\zeta}{2}-\alpha_2\right)+\mathrm{erf}(\alpha_2)\right\}\exp(\alpha_1\zeta)\\ -\alpha_1\exp(\alpha_1^2)\left\{\mathrm{erf}\left(\frac{\zeta}{2}-\alpha_1\right)+\mathrm{erf}(\alpha_1)\right\}\exp(\alpha_2\zeta)\\ -\alpha_2\exp(\alpha_2^2)\{1+\mathrm{erf}(\alpha_2)\}\{\exp(\alpha_1\zeta)-\exp(\alpha_2\zeta)\}\end{array}\right], \tag{38b}$$

$$\omega_1=-2\exp\left(-\frac{\zeta^2}{4}-\delta^*\zeta\right)+2\exp(\alpha_2\zeta) +2\sqrt{\pi}\alpha_1\exp(\alpha_1^2)\left\{\mathrm{erf}\left(\frac{\zeta}{2}-\alpha_1\right)-\mathrm{erf}(-\alpha_1)\right\}\exp(\alpha_2\zeta). \tag{39b}$$

Substitution of c_1 and w_1 in Eq. (17) by Eq. (30) and (34) followed by orthogonalization process reduces the stability equations to the following matrix form:

$$\tau\frac{d\mathbf{a}}{d\tau}=\mathbf{B}\mathbf{a}, \tag{40a}$$

where

$$B_{ij}=-(\lambda_i+k^{*2})\delta_{ij}+\sqrt{\tau}\kappa_i\kappa_jC_{ij}, \tag{40b}$$

$$C_{ij}(k^*)=\int_0^\infty\phi_i(\zeta)\psi_j(k^*, \zeta)d\zeta, \tag{40c}$$

$$\mathbf{a}=[a_1, a_2, a_3, \cdots]^T, \tag{40d}$$

for i, j=1, 2, ⋯. It is stressed that the partial differential Eqs. (16)-(18) are reduced into the system of simultaneous linear ordinary differential Eq. (40) without spatial discretization. Furthermore, the characteristic matrix **B** is normal, i.e. $\mathbf{B}=\mathbf{B}^T$, since $C_{ij}=C_{ji}$ through

$$C_{ij}=\int_0^\infty\psi_i\phi_jd\zeta=-\frac{1}{k^{*2}}\int_0^\infty\psi_i\left\{\exp(\delta^*\zeta)\left(\frac{d^2}{d\zeta^2}+\delta^*\frac{d}{d\zeta}-k^{*2}\right)\psi_j\right\}d\zeta -\int_0^\infty\exp(\delta^*\zeta)\left\{\frac{1}{k^{*2}}\frac{d\psi_i}{d\zeta}\frac{d\psi_j}{d\zeta}+\psi_i\psi_j\right\}d\zeta=C_{ji}. \tag{41}$$

From the basic matrix operation, $\tau(d\mathbf{a}/d\tau)^T=\mathbf{a}^T\mathbf{B}^T$, where $\mathbf{B}^T$ is the transpose of **B**, the growth rate defined in Eq. (32) becomes

$$\sigma^*\tau=\frac{1}{\mathbf{a}^T\mathbf{a}}\mathbf{a}^T\left\{\frac{(\mathbf{B}^T+\mathbf{B})}{2}\right\}\mathbf{a}=\frac{1}{\mathbf{a}^T\mathbf{a}}\mathbf{a}^T(\mathbf{B})\mathbf{a}, \tag{42}$$

since $\mathbf{B}=\mathbf{B}^T$. Through eigen analysis [24,25], it can be shown that

$$\sigma^*\tau=\max\{\mathrm{eig}(\mathbf{B})\}. \tag{43}$$

For the limiting case of $\tau \to 0$, $\mathbf{B}_{ij}=(-\mathrm{i})\delta_{ij}$ and its maximum eigenvalue is -1, i.e. $\sigma^*\tau=-1$, and corresponding eigenvector is $[1, 0, 0, \cdots]^T$, which were already shown in the analysis of initial growth rate (see Eq. (33)).

2. Normal Mode Analysis

As discussed above, the characteristic matrix **B** is normal and therefore, one can suppose the dimensionless amplitude functions of disturbances as [24,25]

$$[w_1(\tau, \zeta), c_1(\tau, \zeta)]=[w^*(k^*, \zeta), c^*(\zeta)]\exp(\sigma^*\tau). \tag{44}$$

Then, the stability equation is obtained from the Eqs. (16)-(18) as

$$(D^2+\delta^*D-k^{*2})w^*=-\exp(-\delta^*\zeta)k^{*2}c^* \tag{45}$$

$$\sigma^*\tau c^*-\frac{1}{\sqrt{\pi}}\sqrt{\tau}w^*\exp\left(-\frac{\zeta^2}{4}\right)=\left(D+\frac{\zeta}{2}D-k^{*2}\right)c^* \tag{46}$$

$$w^*=c^*=0 \text{ at } \zeta=0, \tag{47a}$$

$$w^*\to 0 \text{ and } c^*\to 0 \text{ as } \zeta\to\infty. \tag{47b}$$

The eigenvalue problem of Eqs. (45)-(47) is solved by employing the standard outward shooting scheme [26]. To integrate these stability equations, for a given parameters δ^*, k^* and $\sqrt{\tau}$, we retain the boundary conditions at $\zeta=0$, but replace those at the upper boundary by Dw^* and Dc^* at $\zeta=0$. This is the standard procedure of the outward shooting method. Based on the characteristics of eigenvalue problems, $Dw^*(0)=1$ is set and the eigenvalue $\sigma^*\tau$ should be found instead Once all the values at $\zeta=0$ are provided, this eigenvalue problem can be solved numerically from $\zeta=0$ to the outer boundary with the fourth order Runge-Kutta-Gill method. The values of $\sigma^*\tau$ and $Dc^*(0)$ to satisfy Eq. (47b) are pursued by the Newton-Raphson method.

3. Quasi-steady State Approximation

The quasi-steady state approximation (QSSA) has been applied in solving the similar problems [27-29]. Recently, Nield and Kuznetsov [15] introduced the QSSA, the so-called frozen-time model, to analyze the onset of convection in heterogeneous porous media having transient temperature profiles. Under the QSSA, the amplitude functions of disturbance quantity are expressed as,

$$[w_1(\tau, z), c_1(\tau, z)]=[w_1(z), c_1(z)]\exp(\sigma\tau). \tag{48}$$

Then, with the relation (15), the stability Eqs. (13) and (14) can be reduced as

$$\left(\frac{d^2}{dz^2}-k^2\right)w_1+\frac{\delta d}{Ra}\frac{dw_1}{dz}=-k^2\exp\left(-\frac{\delta d}{Ra}z\right)c_1, \tag{49}$$

$$\sigma c_1=\left(\frac{\partial^2}{\partial z^2}-k^2\right)c_1-w_1\frac{\partial c_0}{\partial z}. \tag{50}$$

under the boundary conditions (11). The outward shooting method explained in the above section can be applied to solve Eqs. (49) and (50).

For the extreme case of very small τ, following Ghesmat et al's [29] approach, Eq. (50) can be approximated as

$$\left(\frac{\partial^2}{\partial z^2}-k^2-\sigma\right)c_1=0 \text{ for } \tau\to 0, \tag{51}$$

and, the following initial growth rate can be obtained:

$$\sigma\to -k^2 \text{ as } \tau\to 0. \tag{52}$$

This simplified solution suggests that regardless of the heterogeneity parameter, the largest growth rates are shifted towards the negative values, i.e., the system is stable.

DIRECT NUMERICAL SIMULATION

1. Formulation

The above linear stability analysis predicts the growth and onset of the instabilities; however, more general information can be obtained by solving Eqs. (1)-(3) directly. Taking the curl of Eq. (2), the following dimensionless equation can be easily obtained:

$$[\nabla\times(f\mathbf{u})]_y=\frac{\partial(fu)}{\partial z}-\frac{\partial(fw)}{\partial x}=-\frac{\partial c}{\partial x}. \tag{53}$$

In addition, by expressing the velocity and concentration fields as $\mathbf{u}=(-\partial\psi/\partial z, 0, \partial\psi/\partial x)$ and $c(\tau, x, z)=c_0(\tau, z)+c_1(\tau, x, z)$, where ψ is a stream function and $c_0(\tau, z)$ is already given in Eq. (8), the field equations for the concentration and the stream function of two-dimensional (2-D) motion in a porous medium reduce to

$$\nabla^2\psi+\frac{\partial \ln f}{\partial z}\frac{\partial\psi}{\partial z}=-f\frac{\partial c_1}{\partial x}, \tag{54}$$

$$\frac{\partial c_1}{\partial\tau}=\nabla^2 c_1-j, \tag{55}$$

$$j=\frac{\partial\psi}{\partial x}\frac{\partial c_0}{\partial z}+\left(\frac{\partial\psi}{\partial x}\frac{\partial c_1}{\partial z}-\frac{\partial\psi}{\partial z}\frac{\partial c_1}{\partial x}\right), \tag{56}$$

The proper boundary conditions for the large Ra system are

$$\psi=c_1=0 \text{ at } z=0 \text{ and } z=Ra \tag{57}$$

To take advantage of the fast Fourier transform (FFT) with consideration of the governing equations and boundary conditions for ψ and c_1, the present problem defined in [0, Ra] can be extended to [−Ra, Ra]by assuming $\tilde{\psi}$ and $\tilde{c}_1$ are the odd expansions of ψ, c_1, and $\tilde{f}$ and $\partial\tilde{c}_0/\partial z$ are the even expansions of f and $\partial c_0/\partial z$,

$$\nabla^2\tilde{\psi}+\frac{\partial \ln\tilde{f}}{\partial z}\frac{\partial\tilde{\psi}}{\partial z}=-\tilde{f}\frac{\partial\tilde{c}_1}{\partial x}, \tag{58}$$

$$\frac{\partial\tilde{c}_1}{\partial\tau}=\nabla^2\tilde{c}_1-\tilde{j}, \tag{59}$$

$$\tilde{j}=\frac{\partial\tilde{\psi}}{\partial x}\frac{\partial\tilde{c}_0}{\partial z}+\left(\frac{\partial\tilde{\psi}}{\partial x}\frac{\partial\tilde{c}_1}{\partial z}-\frac{\partial\tilde{\psi}}{\partial z}\frac{\partial\tilde{c}_1}{\partial x}\right), \tag{60}$$

The proper boundary conditions are

$$\tilde{\psi}=\tilde{c}_1=0 \text{ at } z=\pm Ra. \tag{61}$$

2. Fourier Spectral Method

As discussed, the dominant diffusional operator in the (τ, z)-domain, $\partial^2/\partial z^2$ does not have localized eigenfunctions. So, the spectral method used in the linear stability analysis section cannot be applied in the (τ, z)-domain. Here, Eqs. (58)-(61) are solved by the pseudo-spectral method, which has been used in the similar problems [30-32]. If the physical domain $[0, L_x]\times[-L_z/2, L_z/2]$ is discretized over an equi-spaced mesh of M collocation points in the

x-direction and N collocation points in the z-direction, the discrete Fourier transform (DFT) of the physical quantity ω is

$$\mathcal{F}(\omega)=\hat{\omega}_{p,q}=\frac{1}{\sqrt{MN}}\sum_{m=0}^{M-1}\sum_{n=0}^{N-1}p_{m,n}\exp\{i(k_p x+k_q z)\}, \tag{62}$$

where $k_p=2\pi m/L_x$ and $k_q=2\pi n/L_z$. In the present study, we chose $L_x=L_z=2Ra$. Using the DFT, Eqs. (58) and (59) are transformed into the following ordinary differential equations:

$$\left(k_p^2+k_q^2+\frac{\delta d}{Ra}ik_q\right)\hat{\psi}_{p,q}=\mathcal{F}\left(\tilde{f}\frac{\partial\tilde{c}_1}{\partial x}\right), \tag{63}$$

$$\frac{d\hat{c}_{p,q}}{d\tau}=-(k_p^2+k_q^2)\hat{c}_{p,q}-\hat{j}_{p,q}. \tag{64}$$

After obtaining the Fourier components $\hat{\psi}_{p,q}$ and $\hat{c}_{p,q}$ by solving the above equations, their physical components $\tilde{\psi}(\tau, x, z)$ and $\tilde{c}_1(\tau, x, z)$ were obtained by taking inverse discrete Fourier transform (IDFT) on their Fourier components. Two-dimensional (2-D) DFT and IDFT calculations are conducted using 2-D FFT routine. The solution of the ordinary differential Eq. (64) can be expressed analytically as

$$\hat{c}_{p,q}(\tau+\Delta\tau)=\exp\{(k_p^2+k_q^2)(\tau+\Delta\tau)\}\left[\int_{\tau}^{\tau+\Delta\tau}\exp\{-(k_p^2+k_q^2)\tau'\}\hat{j}_{p,q}d\tau'\right]+\hat{c}_{p,q}(\tau). \tag{65}$$

And, the integral in the above equation is calculated with the Adams-Bashforth predictor-corrector method.

3. Initial Value Problem Approach in Linear Regime

For linear analysis, by neglecting the nonlinear term Eq. (60) can be reduced as

$$\tilde{j}=\frac{\partial\tilde{\psi}}{\partial x}\left(\frac{\partial\tilde{c}_0}{\partial z}\right). \tag{66}$$

And, from the analysis of initial growth rate (see Eq. (30)), the following initial condition is introduced:

$$c_1=\frac{1}{\sqrt{2\sqrt{\pi}}}\zeta_e\exp\left(-\frac{\zeta_2^2}{4}\right)\sin(kx)\ \text{at}\ \tau=\tau_e, \tag{67}$$

where $\zeta_e=z/\sqrt{\tau_e}$. The growth rate is evaluated using the l^2-norm of concentration disturbance defined as

$$|c_1|=\left[\int_0^{l_x}\int_0^{Ra}c_1^2\,dz\,dx\right]^{1/2}, \tag{68}$$

And based on this quantity, the growth rate σ can be defined as

$$\sigma=\frac{1}{|c_1|}\frac{d|c_1|}{d\tau}\approx\frac{1}{\Delta\tau}\ln(|c_1|_{(\tau+\Delta\tau)}/|c_1|_{\tau}). \tag{69}$$

For the various δ/Ra values, Fig. 3 shows a comparison among the conventional QSSA, the present normal mode solution and the numerical calculation results. As shown in Fig. 3, the results of the present study are in very good agreement. In this case, we designate the calculation domain as $[0, \lambda]\times[-100, 100]$ where $\lambda(=2\pi/k)$ is the wavelength with a corresponding wavenumber k, and the initiation time is τ_e=0.01.

4. Direct Numerical Simulation (DNS)

In the previous single mode linear analysis, the wavelength of the disturbances was fixed throughout the simulation. However, we have not observed the nonlinear phenomena such as wavelength selection mechanism in the single-mode analysis. In this section, we set the calculation domain as $[0, 2Ra]\times[-Ra, Ra]$. Through the careful convergence test, Ra=1000 and 2048×2048 collocation points are used unless noted otherwise Since the dominant wavenumber cannot be suggested by the analysis of initial growth rate, the following initial condition is employed in the present simulation:

$$c_1=a_e\frac{1}{\sqrt{2\sqrt{\pi}}}\zeta_e\exp\left(-\frac{\zeta_2^2}{4}\right)\text{rand}(x)\ \text{at}\ \tau=\tau_e, \tag{70}$$

where rand(x) is the pseudo-random number between −1 and 1 with an uniform distribution at the collocation points.

In similar problems, many researchers are interested in the enhancement of dissolution rate due to the instability motion. So, we will consider the rate of dissolution. The non-dimensionalized total gas dissolution flux into the fluid-saturated porous medium, J, can be broken down into two terms, contributions from the base state, J_0, and the convective motion, J_1:

$$J=J_0+J_1. \tag{71}$$

The diffusional flux can be evaluated explicitly from the base concentration profile, Eq. (8), as

$$J_0=-\left.\frac{\partial c_0}{\partial z}\right|_{z=0}=\frac{1}{\sqrt{\pi\tau}}. \tag{72}$$

The flux from the convective motion can be obtained as

$$J_1=\frac{1}{L_x}\int_0^{l_x}\left\{-\left.\frac{\partial c_1}{\partial z}\right|_{z=0}\right\}dx. \tag{73}$$

Here, we set the horizontal extent as L_x=2Ra.

RESULTS AND DISCUSSION

The present analysis of initial growth rate shows that initially the

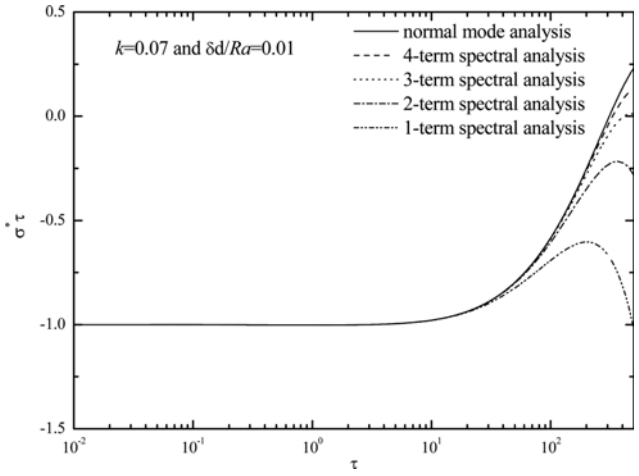

Fig. 2. Temporal evolution of the growth rates obtained from the various methods for the case of k=0.07 and δ/Ra=0.01.

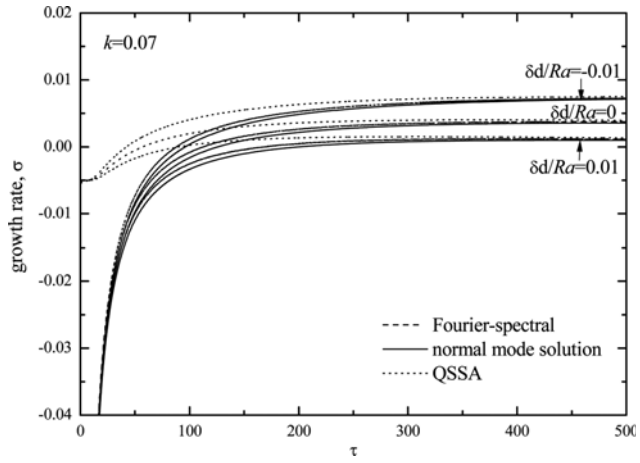

Fig. 3. Comparison of the growth rates obtained from the various methods for the case of k=0.07. For larger Ra, the initial growth rates using the QSSA approach $-k^2$ as $\tau\rightarrow 0$.

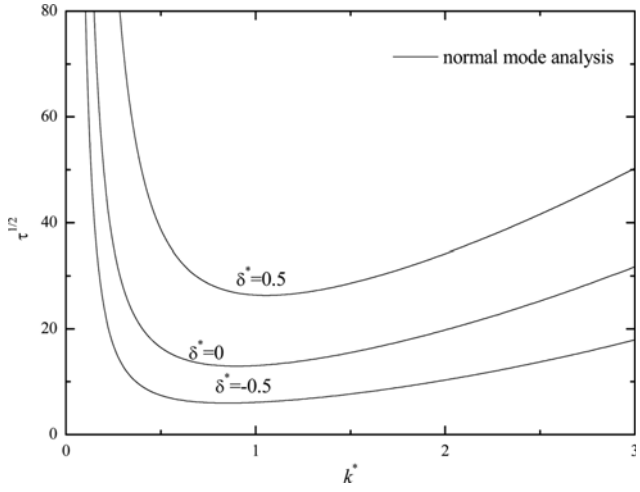

Fig. 4. Neutral stability curves obtained from the normal mode analysis for the semi-infinite case.

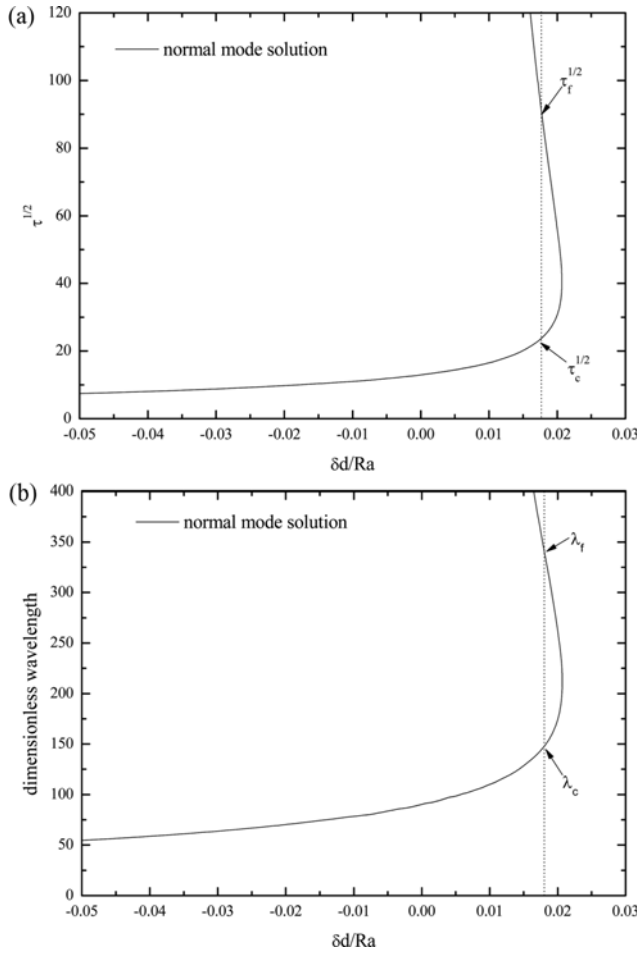

Fig. 5. Effect of the heterogeneity parameter on the critical conditions obtained from the normal mode analysis. (a) critical time and (b) critical wavelength.

system is unconditionally stable regardless of the wavenumber k and the functional form of f at the initial state. Furthermore, the analysis of initial growth rate gives the most unstable disturbance as a deterministic function. For the semi-infinite case of $\sqrt{\tau}$/Ra<<1, the growth rates calculated from the spectral method are compared with the numerical shooting solution under the normal mode analysis in Fig. 2. As shown in the figure, for the limiting case of $\tau\rightarrow 0$, all approximate spectral solution converge to the normal mode solution. However, with increasing τ, the more terms seem to be required.

The neutral stability curves corresponding to $\sigma^*=0$ obtained from the normal mode solution are summarized in Fig. 4. The minimum value of each curve corresponds to the critical condition for the onset of instability. The critical conditions are summarized in Fig. 5. This figure shows that for the case of δ/Ra≤0.02, the instability having the wavelength λ_c onset at τ_c is disappeared after some characteristic time τ_f at which its wavelength is λ_f, and that no instability motion can be expected for δ/Ra>0.02. In the semi-infinite case of small τ, the lower boundary condtion has no effects on the critical condtions: there is no difference between the present dissolution system and the isothermally heated one which has been studied [10]. For the homogeneous case, δ/Ra=0, the present critical conditions are

$$\tau_c=167.547 \text{ and } k_c=0.0695, \tag{73}$$

which are exactly same as those suggested by Selem and Rees [10] and Kim and Choi [19].

For the homogeneous case, δ/Ra=0, we evaluated the effect of the amplitude of the initial disturbance on the total flux, J, and the convective flux, J_1, from the nonlinear DNS studies, and the results are depicted in Fig. 6. In this figure, we plot total flux, J, and the convective flux, J_1, for four different cases with a fixed Rayleigh number of Ra=1000. Without regard to the magnitude of the initial disturbance, diffusion dominates over convection and the disturbances remains in linear region during the initial period. It is interesting that the convective flux, J_1, starts to increase from the critical time obtained from the linear stability analysis: τ_c=167.547. Also, it takes longer time for the nonlinear term to begin to dominate when the initial disturbance is weaker. From now on, we use

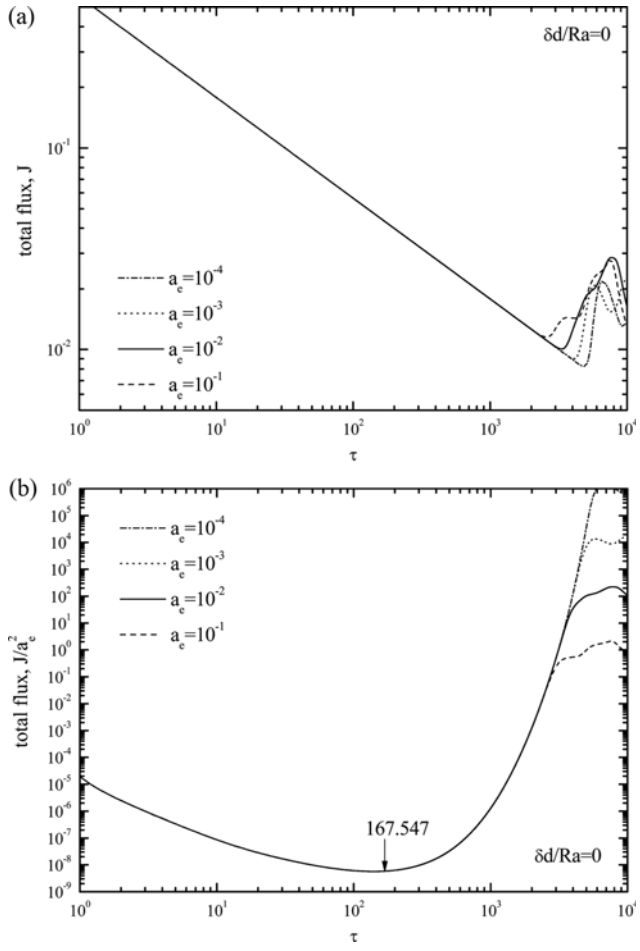

Fig. 6. Effect of the amplitude of the initial disturbance on the temporal evolution of (a) the total flux and (b) the convective for the homogeneous case, i.e., δ/Ra=0.

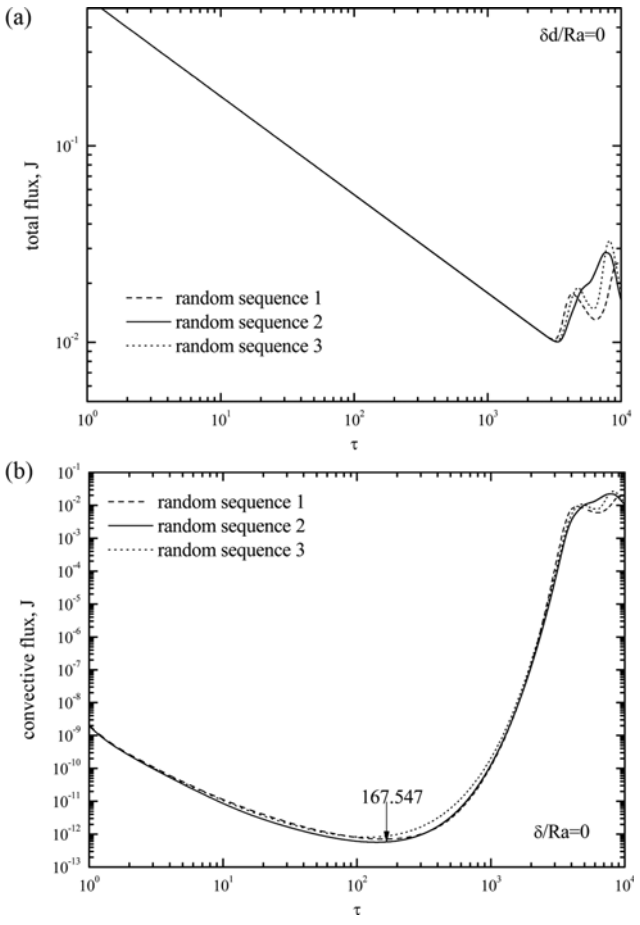

Fig. 7. Effect of the random number sequence of the initial disturbance on the temporal evolution of (a) the total flux and (b) the convective for the homogeneous case, i.e., δ/Ra=0.

Eq. (69) with τ_e=1 and a_e=0.01 as an initial condition. In Fig. 7, we present the effect of random number sequence on the growth rate and the convective flux. It can be seen that the random number sequence has little effect on the growth rate. Without regard to the random number sequence, the nonlinear effects are not apparent until τ=3000. However, it is difficult to characterize the amplitude and shape of initial disturbances for a real physical system.

Now, let us discuss the effect of vertical heterogeneity on the nonlinear growth of instability motion. For a certain random number sequence, the evolution of the convective flux is shown in Fig. 8, where vertical heterogeneity of the permeability in a porous medium plays a critical role in the growth of the instability motion. An important finding from Fig. 8 is that for the case of δ/Ra>0.015, the convective flux continuously decreases as time goes on and therefore, instability motion cannot be expected. This critical value $(\delta d/Ra)_c \approx 0.015$ is more severe than that from the linear theory, $(\delta d/Ra)_c \approx 0.020$ (see Fig. 5). In the linear analysis, the most dangerous disturbance is considered, whereas the horizontal structure of the disturbance is not fixed in the present DNS study. It is presumed that the discrepancy in methodology causes the slight difference between the linear and the non-linear analyses.

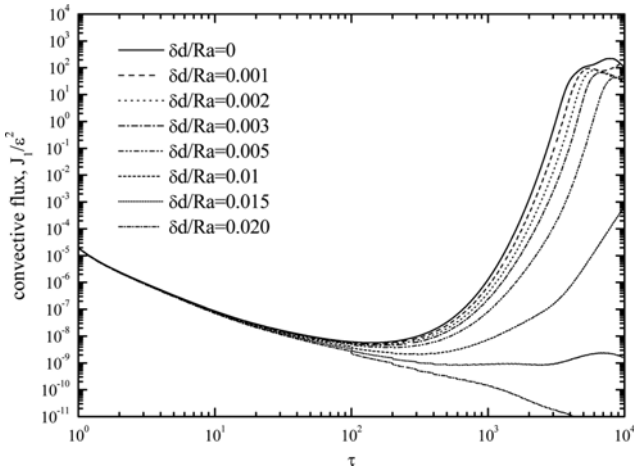

Fig. 8. Effect of the vertical heterogeneity of permeability on the temporal evolution of the convective flux.

For the various values of δd/Ra, total fluxes calculated from the present DNS are summarized in Fig. 9. As shown, the present τ_c obtained from the linear stability theory is much shorter than τ_m at which the total flux shows its minimum. This means that the

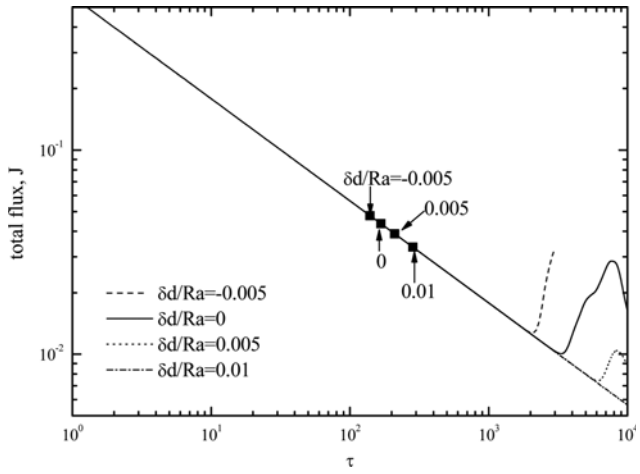

Fig. 9. Effect of the vertical heterogeneity of permeability on the temporal evolution of the total flux. ■ Represents τ_c from the linear stability analysis.

growth period during which the convective motion grows enough to be apparent is much larger than the τ_c. For the cases of δd/Ra=±0.005, the temporal evolution of the concentration field is featured in Fig. 10. The instability grows as fingers and its intensity increases as time goes by. As shown, it is clear that the vertical variation in permeability plays a critical role in the growth of the instability motion.

In the present study, the effect of the vertically-varying permeability on the onset condition of buoyancy-driven convection was analyzed. However, there are many other factors which affect the onset condition, such as the anisotropy of diffusivities, concentration dependent viscosity, geothermal gradient and geochemical reaction. Therefore, many extensions of the present study including double diffusive convection are possible and should be analyzed.

CONCLUSIONS

The critical condition that leads to the onset of convective motion in an initially quiescent, horizontal porous layer was investigated using linear and nonlinear analyses. The linear stability equations were solved using spectral analysis, the normal mode analysis and the quasi-steady state approximation (QSSA). Through the analysis of initial growth rate without the QSSA, we found that initially the system is stable, and identified the most dangerous disturbance deterministically. The vertical variation in permeability changes the stability characteristics quite significantly. The resulting stability criteria are in good agreement with previous theoretical predictions. The nonlinear phenomena such as the increase in the dissolution rate, the symmetry break and the widened structure of fingering were studied through numerical simulations. The present linear and nonlinear analyses may be extended into the various systems where precipitation and geochemical reaction play an important role in dissolution processes.

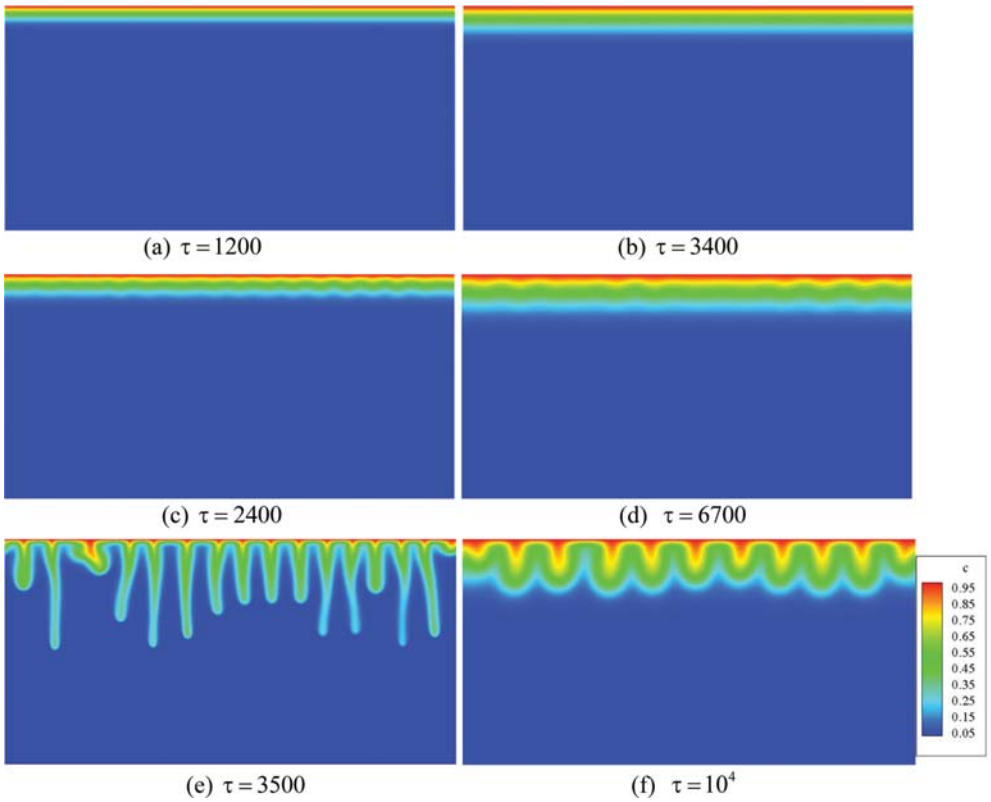

Fig. 10. Temporal evolution of concentration fields for Ra=1000. Left hand side is for δRa=−0.005, and right hand side is for δRa=0.005. Plotting domain is [0, 2000]×[0, 1000].

ACKNOWLEDGEMENT

This research was supported by the Basic Science Research Program through the National Research Foundation of Korea (NRF) funded by the Ministry of Education (NRF-2015R1D1A3A01015798).

REFERENCES

1. C. W. Horton and F. T. Rogers, *J. Appl. Phys.*, **6**, 367 (1945).
2. E. R. Lapwood, *Proc. Camb. Philos. Soc.*, **44**, 508 (1948).
3. D. A. Nield and A. Bejan, *Convection in Porous Media*, 4th Ed., Springer (2013).
4. J.-P. Caltagirone, *Q. J. Mech. Appl. Math.*, **33**, 47 (1980).
5. J. Ennis-King, I. Preston and L. Paterson, *Phys. Fluids*, **17**, 084107 (2005).
6. X. Xu, S. Chen and D. Zhang, *Adv. Water Resour.*, **29**, 397 (2006).
7. H. Hassanzadeh, M. Pooladi-Darvish and D. W. Keith, *Trans. Porous Med.*, **65**, 193 (2006).
8. S. Rapaka, S. Chen, R. J. Pawar, P. H. Stauffer and D. Zhang, *J. Fluid Mech.*, **609**, 285 (2008).
9. A. Riaz, M. Hesse, H. A. Tchelepi and F. M. Orr, *J. Fluid Mech.*, **548**, 87 (2006).
10. A. Selem and D. A. S. Rees, *J. Porous Med.*, **10**, 1 (2007).
11. D. Wessel-Berg, *SIAM J. Appl. Math.*, **70**, 1219 (2009).
12. M. C. Kim and C. K. Choi, *Phys. Fluids*, **19**, 088103 (2007).
13. A. Riaz and Y. Cinar, *J. Petrol. Sci. Eng.*, **124**, 367 (2014).
14. S. Rapaka, R. J. Pawar, P. H. Stauffer, D. Zhang and S. Chen, *J. Fluid Mech.*, **641**, 227 (2009).
15. D. A. Nield and A. V. Kuznetsov, *Transp. Porous Med.*, **85**, 691 (2010).
16. P. Ranganathan, R. Farajzadeh, H. Bruining and P. L. J. Zitha, *Transp. Porous Med.*, **95**, 25 (2012).
17. X.-Z. Kong and M. O. Saar, *Int. J. Greenhouse Gas Control*, **19**, 160 (2013).
18. A. A. Hill and M. R. Morad, *Proc. R. Soc. A*, **470**, 20140373 (2014).
19. M. C. Kim and C. K. Choi, *Korean J. Chem. Eng.*, **32**, 2400 (2015).
20. S. Chandrasekhar, *Hydrodynamic and Hydromagnetic Stability*, Oxford U. P. (1961).
21. A. J. Harfash and A. A. Hill, *Int. J. Heat Mass Transfer*, **72**, 609 (2014).
22. A. J. Harfash, *Transp. Porous Med.*, **102**, 43 (2014).
23. Y. Ben, E. A. Demekhin and H.-C. Chang, *Phys. Fluids*, **14**, 999 (2002).
24. M. C. Kim and C. K. Choi, *Phys. Fluids*, **24**, 044102 (2012).
25. A. C. Slim and T. S. Ramakrishnan, *Phys. Fluids*, **22**, 124103 (2010).
26. M. C. Kim, *Korean J. Chem. Eng.*, **35**(2), 364 (2017).
27. W. Lick, *J. Fluid Mech.*, **21**, 565 (1965).
28. C. T. Tan and G. M. Homsy, *Phys. Fluids*, **29**, 3549 (1986).
29. K. Ghesmat, H. Hassanzadeh and J. Abedi, *J. Fluid Mech.*, **673**, 480 (2011).
30. C. T. Tan and G. M. Homsy, *Phys. Fluids*, **31**, 1330 (1988).
31. W. B. Zimmerman and G. M. Homsy, *Phys. Fluids A*, **4**, 2348 (1992).
32. O. Manickam and G. M. Homsy, *J. Fluid Mech.*, **288**, 75 (1995).